 CMES, vol.82, no.4, pp.215-232, 2011

Numerical Simulation of Melt Filling and Gas Penetration in Gas Assisted Injection Molding

Qiang Li[1], Jie Ouyang[1], Guorong Wu[1] and Xiaoyang Xu[1]

Abstract: The governing equations of two-phase flows including gas and polymer melt are presented, which are solved using finite volume and domain extension methods with SIMPLEC technology. The melt filling and primary gas penetration in gas-assisted injection molding (GAIM) process are simulated, where the Cross-viscosity model is employed to describe the melt rheological behavior, and the CLSVOF(coupled Level Set and Volume of fluid) method is employed to capture the moving interfaces. In order to test and verify the coupled methods, melt filling in a rectangular plate with an insert is simulated, and the numerical results are in good agreement with those of the experiment. As a case study, the melt filling and gas penetration processes in a ring-shaped channel are simulated. The numerical results successfully depict some important phenomena, such as race-tracking effect, corner effect and the flow asymmetry of the gas penetration, which can deepen the understanding and studying of the GAIM process.

Keywords: Gas-assisted injection molding, melt filling, gas penetration, finite volume method, CLSVOF.

1 Introduction

The plastics industry plays an important role in today's manufacturing industry, where gas assisted injection molding (GAIM) is an innovative plastic processing technology [Avery, (2001)], which can reduce the mold cavity pressure-based and avoid forming the structure of rough surfaces generated. Due to plastic product's lower weight, reduce the molding and cooling time, thus GAIM technology has been subject to wider application in the manufacturing industry. The GAIM process includes three parts, i.e. melt filling, primary and secondary gas penetration processes(Fig. 1) [Avery, (2001)]. Recently, the numerical simulation of melt filling and gas penetration processes has been done successfully by many researchers.

[1] chool of Science, Northwestern Polytechnical University, Xi'an 710129, China, jieouyang@nwpu.edu.cn

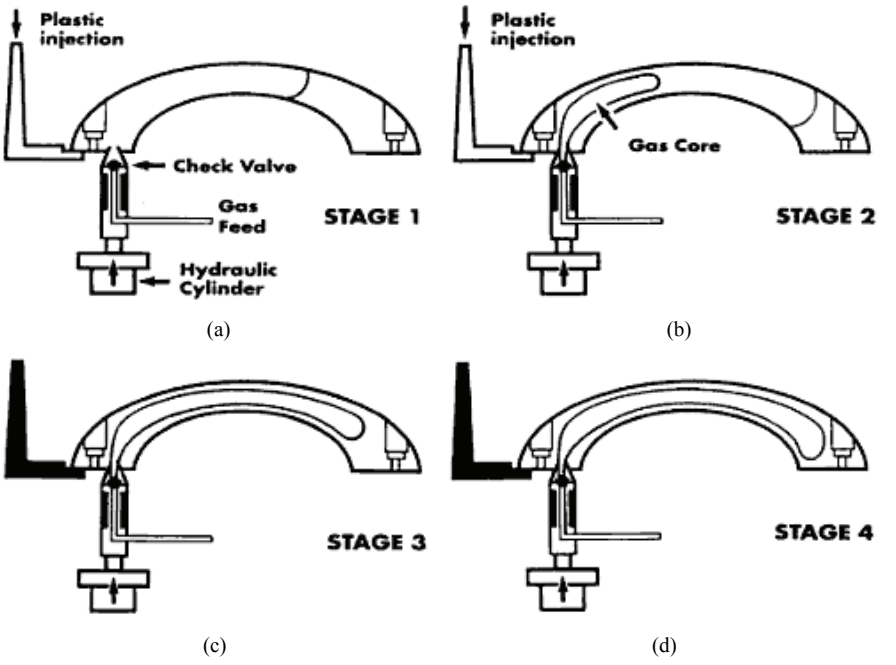

Figure 1: Injection sequence for gas injection into mold: (a) melt injection, (b) gas penetration, (c) primary gas penetration finishing, (d) secondary gas penetration.

Before the gas penetrating, polymer melt is injected into the mold cavity. This process is the same as conventional injection molding (CIM). Zheng et al. (2009) study a numerical scheme for capturing free front during injection molding, and the numerical results show that the Level Set (LS) method can precisely capture the melt front and the LS equations can be well solved by the third-order central WENO scheme. Yang et al. (2010) adopt LS and finite volume methods to simulate viscoelastic fluid mold filling process, and satisfactory results are also obtained.

Since in the gas penetration process the dynamic interaction between gas and melt is very complex, the numerical simulation of GAIM is more difficult than that of CIM. The gas distribution is of great importance to understand and study gas penetration process, thus the gas/melt interface tracking is quite necessary for GAIM, and some research works have been done recently. Llubca and Hétu (2002) present a finite element algorithm for solving GAIM problems and two additional transport equations are employed to track the moving interfaces. Chau and Lin (2006) apply finite volume and volume of fluid (VOF) methods to simulate 3D GAIM pro-

cesses. Polynkin et al. (2005) adopt two pseudo-concentration functions to track the moving interfaces. Zhou et al. (2009) employ the matching asymptotic expansion method to solve the governing equations, while the analytical solution of the gas penetration interface is presented. Chen et al. (2011) apply the Galerkin finite element method discretize the governed equations, and the gas/melt interface is located by VOF method.

In the above interface-tracking methods, the LS and VOF methods are two common methods which are widely used. An advantage of VOF method is the fact that it can conserve the volume of each fluid phase exactly [Park et al. (2009)]. The big disadvantage of VOF method is that it is difficult to smooth the discontinuous physical quantities near the interfaces, because the volume function F is a step function. The LS function ϕ, is defined as a distance function, whose major virtue is that it works in any number of space dimensions, handles topological merging and breaking naturally [Osher and Fedkiw, (2003)]. However, the LS method can not ensure the mass conservation, especially when the interfaces experience severe stretching or tearing. The common disadvantage is the mass loss or gain. To solve the problem, the CLSVOF method which combined the VOF and LS methods have been successfully implemented [Sussman (2000); Son (2002); Son (2003); Sussman (2003); Menard (2007); Yang (2007); Wang (2009)]. Li et al. (2011) apply CLSVOF method to simulate the GAIM process for a door handle, and good results are obtained.

This paper mainly focuses on the numerical simulation of melt injection and primary gas penetration processes. The two-phase flow model which is proposed in [Li et al. (2011)] is adopted to predict the melt filling and gas penetration phenomena, where the Cross-viscosity model is employed to describe the viscous behavior of polymer melt. The governing equations of two-phase flows are solved using finite volume and domain extension methods with SIMPLEC technology. The CLSVOF method [Son (2002); Son (2003)] is adopted to capture the moving interfaces in melt injection and gas penetration processes. The content of this paper is listed as follows. First, the mathematical model is proposed in Section 2. Section 3 presents the numerical implementation of the finite volume and CLSVOF methods. In Section 4 the interface tracking capability of the CLSVOF method is tested and verified by comparing the numerical and experimental results. As a case study, GAIM in a ring-shaped channel is simulated and analyzed in detail. Some conclusions and future research directions conclude this paper.

2 Mathematical Model

2.1 Governing Equations

In the melt filling and gas penetration processes, since the gas velocity is low, both the air-phase and the liquid-phase can be regarded as incompressible flows [Yang et al. (2010); Li et al. (2011)]. The continuity, momentum and energy equations of the incompressible fluids can be written as the unified equations in dimensionless form

$$\frac{\partial \rho}{\partial t} + \nabla \cdot \mathbf{u} = 0 \tag{1}$$

$$\frac{\partial (\rho \mathbf{u})}{\partial t} + \nabla \cdot (\rho \mathbf{u}\mathbf{u}) = -\nabla p + \nabla \cdot (2\eta \mathbf{D}) \tag{2}$$

$$\frac{\partial (\rho CT)}{\partial t} + \nabla \cdot (\rho C \mathbf{u} T) - \nabla \cdot (\kappa \nabla T) = \tau : \nabla \mathbf{u} \tag{3}$$

where $\mathbf{D} = 1/2\left(\nabla \mathbf{u} + \nabla \mathbf{u}^{\mathrm{T}}\right)$ and $\tau = \eta(\phi)(\partial u_i/\partial x_j + \partial u_j/\partial x_i)$.

In two-dimensional case, the governing equations could be written as

$$\frac{\partial \rho}{\partial t} + \frac{\partial (\rho u)}{\partial x} + \frac{\partial (\rho v)}{\partial y} = 0 \tag{4}$$

$$\frac{\partial (\rho u)}{\partial t} + \frac{\partial (\rho uu)}{\partial x} + \frac{\partial (\rho vu)}{\partial y} = -\frac{\partial p}{\partial x} + \frac{\eta}{Re}\left(\frac{\partial^2 u}{\partial x^2} + \frac{\partial^2 u}{\partial y^2}\right) \tag{5}$$

$$\frac{\partial (\rho v)}{\partial t} + \frac{\partial (\rho uv)}{\partial x} + \frac{\partial (\rho vv)}{\partial y} = -\frac{\partial p}{\partial y} + \frac{\eta}{Re}\left(\frac{\partial^2 v}{\partial x^2} + \frac{\partial^2 v}{\partial y^2}\right) \tag{6}$$

$$Pe\left[\frac{\partial (\rho CT)}{\partial t} + \frac{\partial (\rho CuT)}{\partial x} + \frac{\partial (\rho CvT)}{\partial y}\right] - \left(\frac{\partial^2 (\kappa T)}{\partial x^2} + \frac{\partial^2 (\kappa T)}{\partial y^2}\right) = Br \cdot \eta \cdot I \tag{7}$$

where$I = 2(\partial u/\partial x)^2 + 2(\partial v/\partial y)^2 + (\partial u/\partial y + \partial v/\partial x)^2$.$Re = \rho_m UL/\eta_m$ denotes Reynolds number, $Pe = \rho_m C_m UL/\kappa_m$ Peclet number, $Br = \eta_m U^2/\kappa_m T_0$ Brinkman number.

2.2 CLSVOF function and fluid properties

In the CLSVOF method, the interface is reconstructed via a PLIC (Piecewise Linear Interface Construction) scheme from the VOF function, in which the interface normal vector is computed from the LS function [Mark and Elbridge (2000); Son and Hur (2002); Son (2003); Wang et al. (2008)]. Based on the reconstructed interface, the LS function is reinitialized via the geometric operations to conserve

the liquid mass with the aid of the VOF function. The coupling of the LS and VOF methods takes place during the interface reconstruction. The LS and VOF functions are advected using the following equations, respectively

$$\frac{D\Phi}{Dt} = \frac{\partial \Phi}{\partial t} + (\mathbf{u} \cdot \nabla)\Phi = 0 \tag{8}$$

where Φ is ϕ when Eq.(7) is LS function, while Φ is F when Eq.(7) is VOF function. Please see [Son and Hur (2002); Son (2003); Li et al. (2011)] for important details about CLSVOF method.

The melt/air and gas/melt interfaces in melt filling and gas penetration processes are represented by the LS function $\phi(\mathbf{x},t)$[Yang et al. (2010); Li et al. (2011)]. And the sign of $\phi(\mathbf{x},t)$ is that $\phi > 0$ in the melt zone and $\phi < 0$ in the gas zones, respectively.

The LS function can be employed to deal with the discontinuities of density and viscosity near the interface. Each phase has constant density and viscosity, while the fluid properties near the interface have sharp jumps, which are smoothed over a transition band using the LS function

$$\rho = \rho(\phi) = \rho_{\mathrm{g}} + \left(\rho_{\mathrm{m}} - \rho_{\mathrm{g}}\right) H_{\varepsilon}(\phi) \tag{9}$$

$$\eta = \eta(\phi) = \eta_{\mathrm{g}} + \left(\eta_{\mathrm{m}} - \eta_{\mathrm{g}}\right) H_{\varepsilon}(\phi) \tag{10}$$

$$C = C(\phi) = C_g + (C_m - C_g) H_{\varepsilon}(\phi) \tag{11}$$

$$\kappa = \kappa(\phi) = \kappa_g + (\kappa_m - \kappa_g) H_{\varepsilon}(\phi) \tag{12}$$

where ρ, η, C and κ are density, viscosity, thermal capacity and conductivity, respectively. The subscript g and m represent gas and melt, respectively. The smoothed Heaviside function $H_{\varepsilon}(\phi)$ is

$$H_{\varepsilon}(\phi) = \begin{cases} 0 & if \ \ \phi < -\varepsilon \\ \frac{1}{2}\left[1 + \frac{\phi}{\varepsilon} + \frac{1}{\pi}\sin\left(\frac{\pi\phi}{\varepsilon}\right)\right] & if \ \ |\phi| \le \varepsilon \\ 1 & if \ \ \phi > \varepsilon \end{cases} \tag{13}$$

where ε is a parameter related to the interface thickness, and $\varepsilon = 1.5\Delta x$ in this paper. Δx is the grid width along the x direction.

In melt filling and gas penetration process, the Cross-viscosity model is chosen to describe the rheological property of the polymer melt in this paper [Yang et al. (2010); Li et al. (2011); Chau (2008)].

$$\eta(T, \dot{\gamma}, p) = \frac{\eta_0(T, p)}{1 + \left(\eta_0 \dot{\gamma}/\tau^*\right)^{1-n}} \tag{14}$$

where τ^* is the model constant that shows the shear stress rate, n is the model constant which symbolizes the pseudoplastic behavior slope of the melt as $(1-n)$, η_0 is the melt viscosity under zero-shear-rate conditions. η_0 can be expressed as Arrhenius formula

$$\eta_0(T,p) = B\exp\left(\frac{T_b}{T}\right)\exp(\beta p) \tag{15}$$

Eq. (14) is 5-parameter model, where B, T_b and β are material parameters.

Another formula of η_0 is known as Cross-WLF model, or 7-parameter model,

$$\eta_0 = D_1\exp\left(-\frac{A_1(T-T^*)}{A_2+(T-T^*)}\right) \tag{16}$$

where $T^* = D_2 + D_3 \cdot P$, $A_2 = \tilde{A}_2 + D_3 \cdot P$, and D_1, D_2, D_3, A_1 and A_2 are all material parameters.

3 Numerical implementation

3.1 Governing equations solver and Domain extension method

The governing equations are discretized by the finite volume method on the non-staggered meshes [Yang et al. (2010); Li et al. (2011)]. To solve the problem of the pressure-velocity decoupling, we employ SIMPLEC (semi-implicit method for pressure linked equations consistent) method and Momentum Interpolation (MI) on the collocated grids [Yang et al. (2010); Li et al. (2011)].

Generally, in order to solve irregular domain problems, the body fitted or unstructured grids could be used, but a lot of extra programming work will be needed. Domain extension method is an alternative technology which can be convenient to implement [Nie et al. (2002); Korichi et al. (2009)]. Thus, the computational domain is extended to the minimum rectangle which contains the irregular region. In the solid region which is inside the rectangle and outside the irregular region, the dynamic viscosity is set to be a very large value for momentum equation (such as 10^{20}), while thermal conductivity is set to be a very small value for energy equation (such as 10^{-20}).

Another issue that should be concerned is how to distinguish the inside and outside regions. Based on LS function, this paper proposes a simple method to solve the problem. Take Fig.2 for example, the ring-shaped channel is the real mold cavity (the blank area), which can be extended to a rectangle area by defining a shape-level

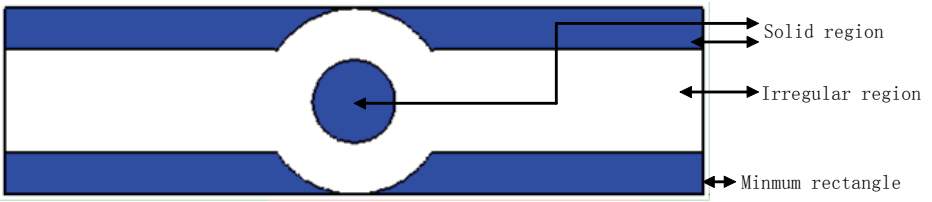

Figure 2: Schematic diagram of Domain extension method.

set function as follows:

$$\Phi^*_{i,j} = \min(R - \sqrt{(x_i - x_1)^2 + (y_j - y_1)^2}, \sqrt{(x_i - x_2)^2 + (y_j - y_2)^2} - r) \quad (x_i \in [0,a]\,,\ y_j \in [0,b]) \tag{17}$$

$$\Phi_{i,j} = \min(\Phi^*_{i,j},\ y_j - y_3,\ y_4 - y_j) \quad (x_i \in [0,c] \text{ or } x_i \in [d,a]) \tag{18}$$

where (x_1, y_1) and (x_2, y_2) are center coordinates of the larger and smaller circles, respectively. R and r are radii of the larger and smaller circles, respectively. a and b are the lengths of the two sides of the rectangle. c and d are the horizontal ordinates of the crossing points of the ring-shaped channel and the straight pipelines. y_3 and y_4 are vertical coordinates of the straight pipelines. According to the shape-level set function $\Phi_{i,j}$, which satisfies that $\Phi_{i,j} > 0$ in the ring-shaped channel and $\Phi_{i,j} < 0$ in the extended regions. Thus, the shape-level set function can be employed to not only define the mold cavity size, but also distinguish the inside and outside regions, which can reduce programming difficulty greatly.

3.2 CLSVOF solver

The LS advection function belongs to the Hamilton-Jacobi equations, which is discretized by the finite difference method, where the spatial derivatives are discretized by the fifth-order WENO (weighted essentially non-oscillatory) scheme, and the temporal derivatives are discretized by the third-order TVD-R-K (total variation diminishing Runge-Kutta) scheme [Yang et al. (2010), Li et al. (2011)].

To solve the VOF function F, the flux-splitting algorithm used by Sussman and Puckett [Nie et al. (2002)] is adopted. Son and Hur (2002), Son (2003) have described the VOF advection algorithm very clearly. In these papers$s$ is a parameter related to the shortest distance from the origin (See Son (2003) for details). Since the normal vector is estimated from the LS function, i.e.$\mathbf{n} = \nabla\phi/|\nabla\phi|$, s is just

the shortest distance from the origin. If s and $\mathbf{n}$ are given, Fcan be calculated immediately, and vice versa [Son and Hur (2002); Son (2003)].

4 Results and analysis

4.1 Melt filling in a rectangular plate with an insert

The physical properties of gas and melt, such as the density and viscosity, differ greatly. In order to validate the interface tracking capability of the CLSVOF method for large-density ratio and large-viscosity ratio two-phase flow problem, melt filling process is simulated in a rectangular plate with an insert. Table 1 summarizes the constants of employed Cross-WLF model for the injected melt, named ABS (Acrylonitrile Butadiene Styrene). The size of the rectangular plate with an insert is shown in Fig. 3. The maximum injection pressure and the maximum velocity are 150MPa and 90cm^3/s, respectively. And the melt and cavity temperatures are 498K and 343K, respectively [Yu (2004)].

Table 1: Material properties and Cross–WLF model constants for ABS.

Parameters	Values	Parameters	Values
Apparent density $\rho\ (kg/m^3)$	931.7	$\tau^*\ (Pa)$	5200.2
Specific heat $c_p\ (J/kg\cdot K)$	1900	$\eta_g\ (Pa\ s)$	8.643×10^{17}
Thermal conductivity $k\ (W/m\cdot K)$	0.13	C_1^g	37.15
n	0.351	$C_2^g\ (K)$	51.6

The numerical and experimental results are shown in Fig. 4. From Fig. 4 it is clear that the melt fronts predicted by CLSVOF method are in good agreement with the experimental ones [Yu (2004)], which also demonstrate that the CLSVOF method can do well for capturing the moving interface in melt injection process.

4.2 Melt filling and gas penetration in a ring-shaped channel

4.2.1 Melt filling in a ring-shaped channel

Melt filling process in a ring-shaped channel is simulated, and the channel size is illustrated in Fig. 5. Polystyrene (Polyrex PG-33) [Chau and Lin (2006)] is selected as experimental polymer in this paper. Materials constants are listed in Table 2. And the melt and cavity temperatures are 503K and 323K, respectively. The computational domain is 13.6×3.6, and a uniform grid of 136×36 is used. The initial melt front is set to be a little semi-circle, and the initial injection velocity is 10. The melt-air interfaces are shown in Fig. 6. The melt goes alone the channel before arriving at the round wall. Then the melt bifurcates into two narrow rounded

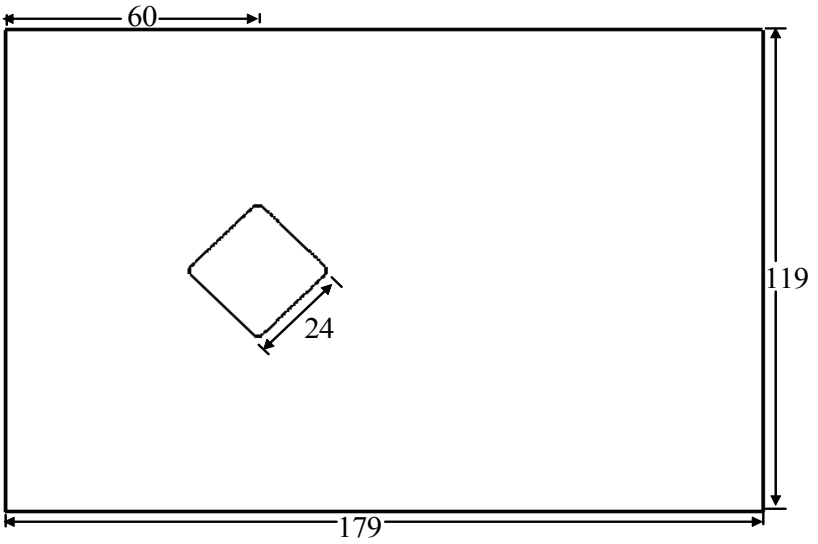

Figure 3: The size of the rectangular plate with an insert.

channels. Because the inner length is shorter than the outer length of ring-shaped channel, the two streams of melt meet at the inner side of the channel (Fig. 6), which is so-called race-tracking effect[Chau and Lin (2006)]. At last the melt front is in the arc shape until the mould cavity is filled with melt.

Table 2: Material properties and Cross–WLF model constants for PS.

Parameter	Value	Parameter	Value
$\rho(kg/m^3)$	948.15	$D_1(Pa\cdot s)$	2.68×10^{11}
$C_v(J/kg\cdot K)$	2100	$D_2(K)$	373.1
$\kappa(W/m\cdot K)$	0.18	$D_3(Pa/K)$	0.0
n	0.2749		25.88
$\tau^*(Pa)$	20020	$\tilde{A}_2(K)$	51.6

Fig. 7 shows the melt velocity vectors at different time. From Fig. 7 it is obvious that the melt velocity decreases from the middle to the wall of the channel, which also illustrates that the finite volume and domain extension methods could deal with irregular boundary problems well. The fountain flow phenomenon can be seen clearly at the melt front, as is illustrated in Fig. 7(d).

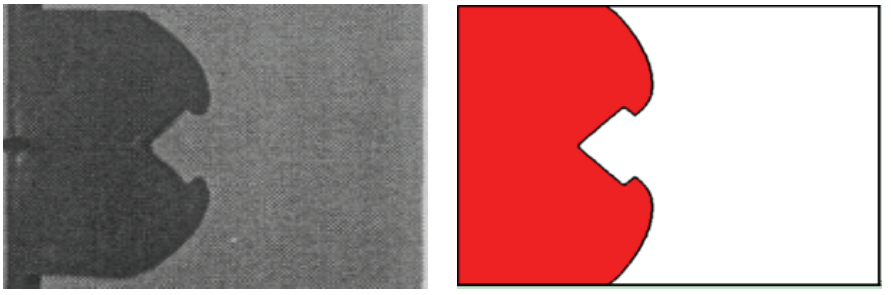

(a) t=0.4s

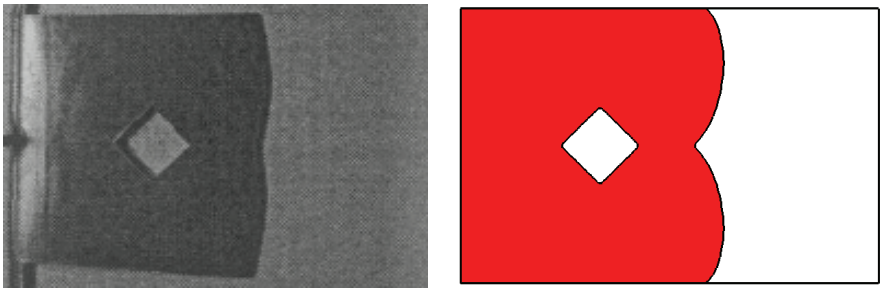

(b) t=0.5s

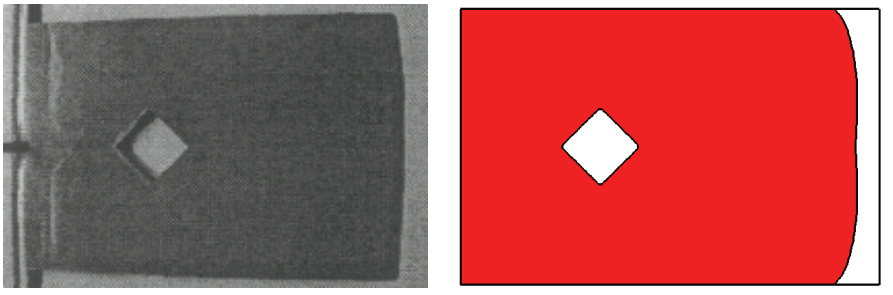

(c)t=1.0s

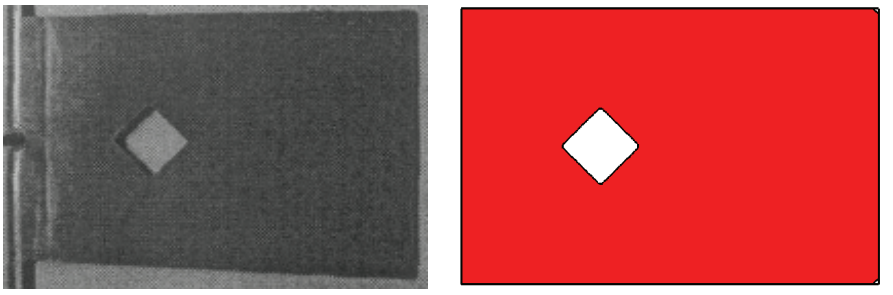

(d)t=1.3s

Figure 4: The melt front at different time: t=0.4s, 0.5s, 1.0s, 1.3s. Left: experimental results; Right: numerical results.

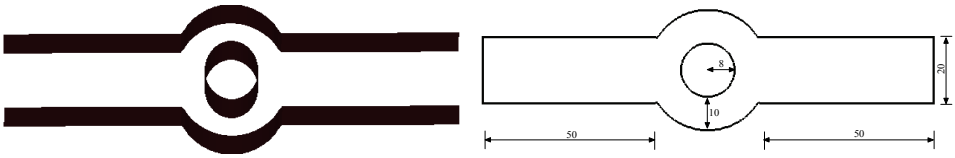

Figure 5: The size of the ring-shaped channel. Left: 3D shapes, Right: mid-plane.

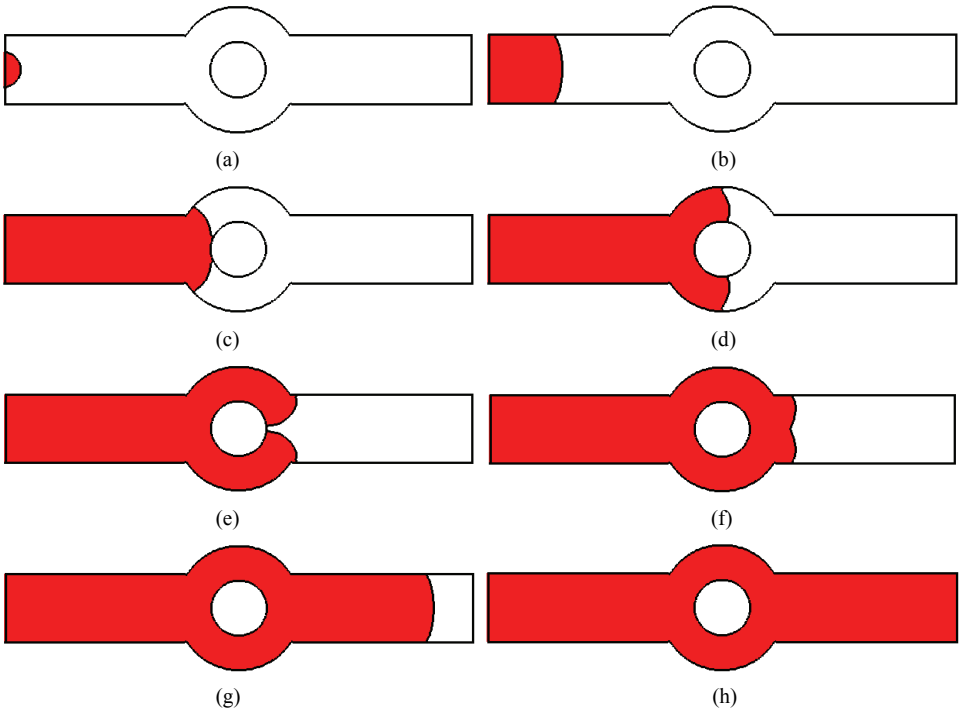

Figure 6: The melt front in the ring-shaped channel at different time: (a) t=0.0, (b) t=3.3, (c) t=9.0, (d) t=10.8, (e) t=13.2, (f) t=14.6, (g) t=19.2, (h) t=21.0.

4.2.2 Gas penetration in a ring-shaped channel

After the full-shot (melt filling) process, the gas is injected into polymer melt in the ring-shaped channel. The gas pressure is chosen as 11764 in the dimensionless form. The initial gas/melt interface is set to be a little circle, as is illustrated in Fig. 8(a). Then the gas bubble becomes bigger and goes ahead along the channel. When

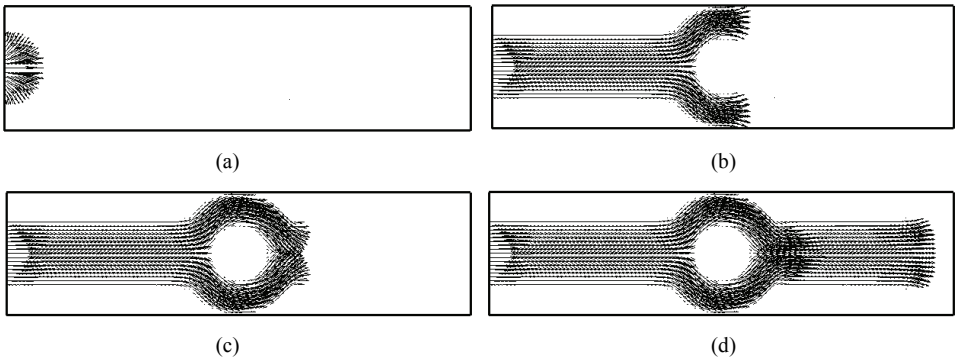

Figure 7: The melt velocity vectors at different time: (a) t=0.9, (b) t=3.3, (c) t=13.2, (d) t=19.2.

it expands to some degree, the bubble goes along the channel without expending (Fig. 8(c)). Fig. 8(d) shows the bubble develops into two branches, and the flow asymmetry phenomenon looms. After it has turned around the circle, the flow asymmetry phenomenon becomes more apparent (Fig. 8(e)). Fig. 8(f) displays the final gas bubble shape at t=18.3. Moreover, when the gas goes through the ring-shaped channel, gas bubble is deflected to the inner channel wall, which is the so-called corner effect [Chau and Lin (2006)].

Fig. 9 shows the comparison of numerical and the experimental results at different time. It is obvious that the flow asymmetry phenomena are in good agreement with the experimental results in [Chau and Lin (2006)].

The predicted bubble shapes at t=18.3 with three different grid sizes are shown in Fig. 10. It can be seen clearly that the asymmetry phenomenon of gas penetration also occurs for finer mesh size, and the gas bubble shapes are almost the same under the three grids. Therefore, it could draw the conclusion that this asymmetry of gas penetration is an intrinsic phenomenon, which is independent on the computational grids.

Fig. 11 illustrates the pressure distributions and melt velocity at different time, where the melt pressure shows zonal distribution, and the melt velocity is large near the gas/melt interface.

In order to study how the geometry affect the gas bubble shapes, four different centre coordinates of the internal circle are chosen, i.e. (6.8, 1.78), (6.8, 1.771), (6.8, 1.77) and (6.8, 1.75). Fig. 12 shows the bubble appearances at t=18.3 for four different centre coordinates. As the centre of the inner circle moves down, the asym-

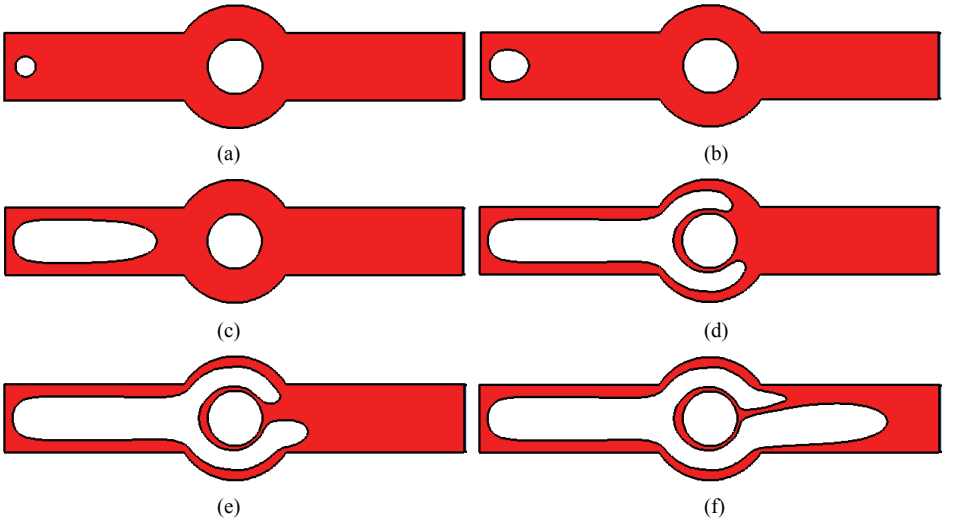

Figure 8: The melt front in the ring-shaped channel at different time: (a) t=0.0, (b) t=1.2, (c) t=7.2, (d) t=13.8, (e) t=15.3, (f) t=18.3.

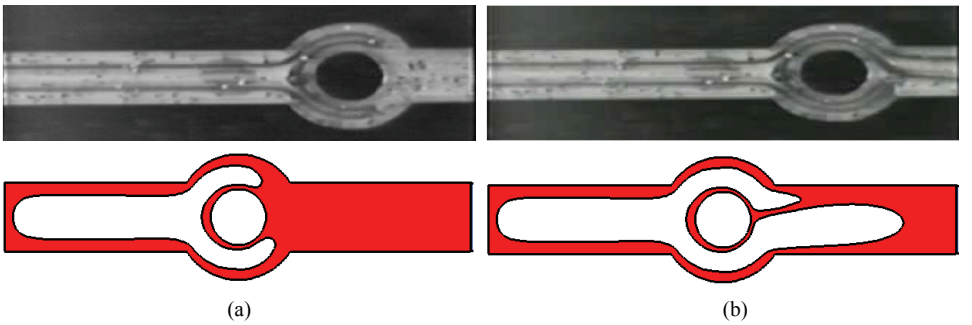

Figure 9: Comparison of the numerical and the experimental results at different time: (a) t=13.8, (b) t=18.3.

metry phenomena change greatly. From Fig. 12(b)∼(c), the centre is just moved down 0.001(=0.01Δx), but the bubble shapes are significantly different. When the centre moves to (6.8, 1.75), i.e. the centre is just moved down 0.05(=0.5Δx), the gas bubble shape is just opposite to that for point (6.8, 1.8). It is easy to know that the geometric dimension affects the bubble appearances greatly and the dynamic interaction between gas and melt is very complex, both of which could lead to the

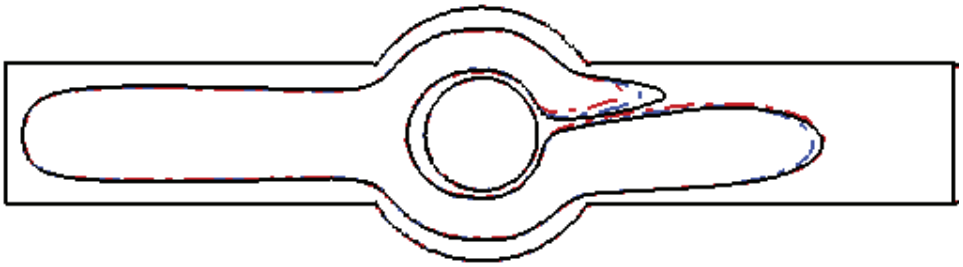

Figure 10: Predicted bubble shapes at t=18.3 with different grid sizes: (a) 136×36(DashDot line) (b) 204×54(DashDotDot line) (c) 272×72(solid line).

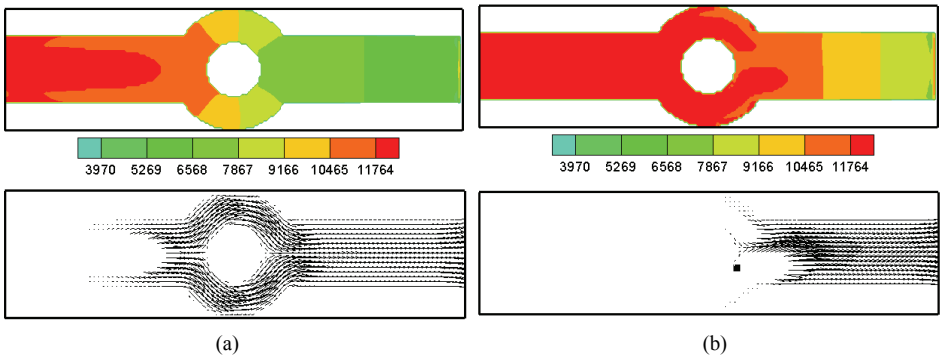

Figure 11: The pressure distributions (up) and melt velocity (down) at different time: (a) t=7.2, (b) t=15.3.

asymmetry phenomenon of gas penetration.

4.2.3 3D gas penetration in a ring-shaped channel

In order to better study the asymmetry phenomenon of gas penetration, the numerical simulation is extended to three-dimensional simulation. The mold cavity size is show in Fig. 5, where the thickness is 2. And the other parameters are the same as Section 4.2.1. Fig. 13 shows the bubble appearance in the ring-shaped channel. From Fig. 13 it is clear that the asymmetry phenomenon also happens in three-dimensional case. It should be noticed that the three-dimensional asymmetry phenomenon is different from the two-dimensional one. The two-dimensional asymmetry phenomenon is that the under branch bubble is longer than the upper, while the reverse is true in three-dimensional case: the upper branch bubble is

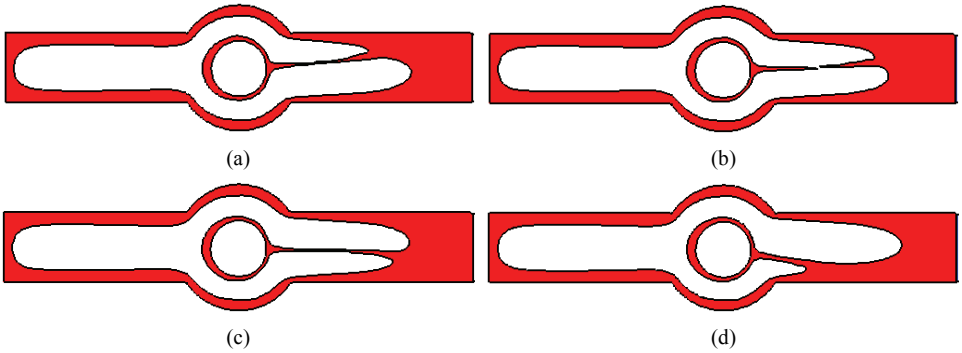

Figure 12: The bubble appearances at t=18.3 for different centre coordinates: (a) (6.8, 1.78), (b) (6.8, 1.771), (c) (6.8, 1.77), (d) (6.8, 1.75).

longer than the under. The two-dimensional and three-dimensional results can be attributable to a small calculation error. The numerical results can explain asymmetry phenomenon in engineering due to a minor disturbance from mold cavity size. Bubble asymmetry phenomenon could lead to unsuccessful gas penetration.

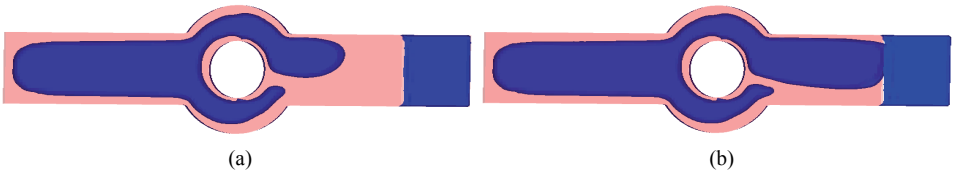

Figure 13: The bubble appearances at different time: (a) t=15.5, (b) t=18.3.

5 Conclusions

This paper presents a mathematical model, which can be applied to the melt filling and gas penetration in GAIM process. Because the dynamic interaction of gas and melt is very complex, the numerical simulation of gas penetration is more difficult than that of melt filling, in which interface capturing is of critical importance to study and optimize the GAIM process. Here the CLSVOF method is adopted to track the moving interfaces. And the conclusions can be drawn as follows.

1. In the domain extension method, a shape-level set function, which can reduce programming difficulty greatly, is proposed to describe the mold cavity size and distinguish the mold cavity and the extended regions.

2. Compared with the experimental results for melt filling process in rectangular plate with an insert, the numerical results show that the finite volume and domain extension methods with SIMPLEC technique can simulate the melt filling process in complex cavity well, and the CLSVOF method could capture the moving interface much accurately.

3. The melt filling and gas penetration processes in a ring-shaped channel is simulated. The flow phenomena, such as race-tracking effect and fountain flow in the full-shot process, the corner effect and flow asymmetry of gas penetration in gas penetration process, could be seen clearly, respectively. To explore the reason of the asymmetry phenomena, numerical simulations under different computational grids are done to study mesh convergence. The numerical results show that the asymmetry of gas penetration is an intrinsic phenomenon, which is independent on the computational grids. Then the symmetrical structure is changed slightly in geometry, while the asymmetry phenomena vary greatly. And the 3D numerical results also depict asymmetry phenomena. So, we can obtain the conclusion that the geometric dimension affects the bubble appearances greatly and the dynamic interaction between gas and melt is very complex, both of which could explain why the asymmetry phenomenon of gas penetration happens.

All the above phenomena obtained by the numerical simulation are of practical importance to deepen the understanding of GAIM processes and optimize the equipment design.

Acknowledgement: All the authors would like to acknowledge the National Natural Science Foundation of China (10871159), the National Basic Research Program of China (2005CB321704) and National key Basic Research Program of China (2012CB025903).

References

Avery, J. (2001): Gas-assist injection molding: Principles and Applications. Hanser.

Chau, S.W. (2008): Three-dimensional simulation of primary and secondary penetration in a clip-shaped square tube during a gas assisted injection molding process. *Polymer Engineering & Science*, vol. 48, no. 9, pp. 1801–1814.

Chau, S.W.; Lin, Y.W. (2006): Three-dimensional simulation of melt filling and gas penetration in gas-assisted injection molding process using a finite volume formulation, *Journal of Polymer Engineering*. Vol. 26, no. 5, pp. 431–450.

Chen, W; Zhou, X.H.; Han, X.H. (2011): Computing Gas/Melt Free Interface of Gas-Assisted Injection Molding. *The International Journal of Advanced Manufacturing Technology*, vol. 52, no. 5-8, pp. 521–529.

Korichi, A; Oufer, L; Polidori, G. (2009): Heat transfer enhancement in self-sustained oscillatory flow in a grooved channel with oblique plates. *International Journal of Heat and Mass Transfer*, vol. 52, no. 5–6, pp. 1138–1148.

Li, Q.; Ouyang, J.; Yang, B.X.; Jiang. T. (2011): Modelling and simulation of moving interfaces in gas-assisted injection moulding process. *Applied Mathematical Modelling*, vol. 35, no. 1, pp. 257–275.

Li, Q.; Ouyang, J.; Li, X.J.; Wu, G.R.; Yang, B.X. (2011): Numerical Simulation of Gas-assisted Injection Molding Process for A Door Handle. *CMES: Computer Modeling in Engineering & Sciences*, vol. 74, no. 4, pp. 247–267.

Llubca, F.; Hétu, J.F. (2002): Three-dimensional finite element solution of gas-assisted injection moulding. *International Journal for Numerical Methods in Engineering*, vol. 53, no. 8, pp. 2003–2017.

Menard, T.; Tanguy, S.; Berlemont, A. (2007): Coupling level set/VOF/ghost fluid methods: validation and application to 3D simulation of the primary break-up of a liquid jet. *International Journal of Multiphase Flow*, vol. 33, no. 5, pp. 510–524.

Nie, J.H.; Armaly, B.F. (2002): Three-dimensional convective flow adjacent to backward-facing step-effects of step height. *International Journal of Heat and Mass Transfer*, vol. 45, no. 12, pp. 2431–2438.

Osher, A.; Fedkiw, R. (2003): Level Set Methods and Dynamic Implicit Surfaces. Springer.

Polynkin, A.; Pittman, J.F.T.; Sienz, J. (2005): Gas assisted injection molding of a handle: three-dimensional simulation and experimental verification. *Polymer Engineering and Science*, vol. 45, no. 8, pp. 1049–1058.

Park, I.R.; Kim, K.S.; Kim, J.; Van, S.H. (2009): A volume-of-fluid method for incompressible free surface flows. *International Journal for Numerical Methods in Fluids*, vol. 61, no. 12, pp. 1331–1362.

Son, G. (2003): Efficient Implementation of a Coupled Level-Set and Volume-of-Fluid Method for Three-Dimensional Incompressible Two-phase Flows. *Numerical Heat Transfer* (Part B), vol. 43, no. 6, pp. 549–565.

Son, G.; Hur, N. (2002): A Coupled Level Set and Volume-of-Fluid Method for Buoyancy-Driven Motion of Fluid Praticles. *Numerical Heat Transfer* (Part B), vol. 42, no. 6, pp. 523–542.

Sussman, M. (2003): A second order coupled level set and volume of fluid method for computing growth and collapse of vapor bubbles. *Journal of Computational Physics*, vol. 187, no. 1, pp. 110–136.

Sussman, M.; Puckett, E.G. (2000): A Coupled Level Set and Volume-of-Fluid

method for computing 3D and axisymmetric incompressible two phase flows. *Journal of Computational Physics*, vol. 162, no. 2, pp. 301–337.

Wang, Z.Y.; Yang, J.; Koo, B.; Stern, F. (2009): A coupled level set and volume-of-fluid method for sharp interface simulation of plunging breaking waves. *International Journal of Multiphase Flow*, vol. 35, no. 3, pp. 227–246.

Yang, B.X.; Ouyang, J.; Li, Q.; Zhao, Z.F.; Liu, C.T. (2010): Modeling and simulation of the viscoelastic fluid mold filling process by Level Set method. *Journal of Non-Newtonian Fluid Mechanics*, vol. 165, no. 19-20, pp. 1275–1293.

Yang, J.; Stern, F. (2007): A sharp interface method for two-phase flows interacting with moving bodies. In: 18th AIAA Computational Fluid Dynamics Conference, Miami, FL, USA, AIAA-2007-4578.

Yu, X.R. (2004): Study and Application of Design Optimization for Injection Molding [D] (China). Zhengzhou: Zhengzhou University.

Zheng, S.; Ouyang, J.; Zhang, L.; Zhao, Z. (2009): Research on a Numerical Scheme for Capturing Free Front during Injection Molding. *Polymer-Plastics Technology and Engineering*, vol. 48, no. 4, pp. 446–454.

Zhou, H.M; Zhang, H.; Li, D.Q. (2009): Modeling and Solution for Gas Penetration of Gas-Assisted Injection Molding. *CMES: Computer Modeling in Engineering & Sciences*, vol. 46, no. 3, pp. 209–220.